Self-activated reversibility in the magnetically induced reorientation of martensitic variants in ferromagnetic Ni-Mn-Ga films

Yuepeng Zhang (张跃鹏),[1] R. A. Hughes,[2,*] J. F. Britten,[3] J. S. Preston,[2,4] G. A. Botton,[1,2] and M. Niewczas[1,2,†]

[1]*Department of Materials Science and Engineering, McMaster University, Hamilton, Ontario, Canada L8S 4L7*

[2]*Brockhouse Institute for Materials Research, McMaster University, Hamilton, Ontario, Canada L8S 4M1*

[3]*McMaster Analytical X-ray Diffraction Facility, McMaster University, Hamilton, Ontario, Canada L8S 4L7*

[4]*Department of Engineering Physics, McMaster University, Hamilton, Ontario, Canada L8S 4L7*

(Received 11 June 2009; revised manuscript received 17 December 2009; published 5 February 2010)

Magnetically induced reorientation (MIR) of twin variants for [101]-oriented martensite has been studied for Ni-Mn-Ga thin films deposited on (001) YSZ substrates. The MIR effect displayed by these films is self-reversible, is characterized by a small increase in the magnetization, and shows a temperature-dependent activation field. These properties can be described in terms of a magnetic microstructure comprised of MIR-active and MIR-inactive twin variants, where the degree of activity depends on the relative orientations of the externally applied magnetic field and the easy axis of the magnetization of the variants. The MIR-active variants are responsible for the detwinning, while the MIR-inactive variants exert a restoring force on the MIR-active variants as they reorient. This interplay between the active and inactive variants is highly advantageous as it allows for the complete self-activation of the reversible MIR effect, a response which is desired for actuation applications. The results further demonstrate that the magnetic domain structure formed in the films is inherited from a substrate-induced crystallographic texture and microstructure. It is also suggested that a tailored MIR response could prove possible through an optimization of the film texture and microstructure.

DOI: 10.1103/PhysRevB.81.054406 PACS number(s): 75.80.+q, 68.60.−p, 62.20.fg, 68.55.−a

I. INTRODUCTION

The ferromagnetic Ni-Mn-Ga alloys belong to a group of shape memory materials, which can generate macroscopic strains upon exposure to a magnetic field of sufficient magnitude.[1] The effect relies upon twin-boundary motion within a martensitic structure. The motion occurs when the difference in the magnetic energy, due to the various orientations of the magnetic moments in twin related variants, exceeds the mechanical energy needed for the displacements of the atoms in the vicinity of the twin boundary. This magnetically induced twin variant reorientation (MIR) gives rise to both an abrupt increase in the magnetization and shape changes.[2] The optimization of the MIR effect has yielded bulk materials exhibiting magnetic field induced strains of ~9.5%,[3] a value significantly larger than the strains observed in fast-response piezoelectric[4,5] and magnetostrictive materials.[6]

While the MIR induced strain in Ni-Mn-Ga single crystals is found to be quite large, the process itself is not self-reversible.[7] Fully reversible strain is, however, obtained through the application of a mechanical restoring force applied in a direction perpendicular to the magnetic field direction.[8–10] Through this means a reversible strain of 6% was obtained in a single crystal of Ni-Mn-Ga (Ref. 9) when an external stress of 1 MPa was applied. Straka *et al.*[10] presented a criterion for strain reversibility during a MIR effect. The criterion requires that the external stress be larger than the twinning stress but smaller than the difference between the twinning stress and the stress exerted by the magnetic field.[10] It has also been determined that the minimum magnetic field required to activate the MIR process increases with decreasing temperature due to a lower twin-boundary mobility.[11–15]

While considerable progress has been made in understanding the MIR effect in bulk Ni-Mn-Ga materials, advances in thin-film properties have been slow. A vast majority of the results available in the literature reveal that films affixed to a rigid substrate show no discernable MIR effect, even though they exhibit a well-defined martensitic transformation. Recent advances, however, have resulted in the deposition of films exhibiting a partial MIR effect.[16–20] In contrast to single crystals, the MIR effect in these films showed reversibility even in the absence of external stresses.[16,17,19,20] The unique nature of the response was attributed to the fact that films are clamped to the substrate.[16] Because of this, a film, unlike its single-crystal counterpart, must reorient in a manner which preserves its overall in-plane dimensions. Recognizing this constraint, Thomas *et al.*[16] described a mode by which the observed reorientation could take place for orthorhombic films with a grain structure containing {100}-oriented grains. In this mode the variant reorientation was facilitated by having the fraction of unit cells with the *b* axis parallel to the field increased at the expense of the unit cells with the *a* axis and *c* axis in the field direction. In this manner, the overall size would be conserved since two *b* axis lattice parameters are approximately equal to the sum of the *a*- and *c*-axis lattice parameters. The reorientation was attributed to an overall energy reduction in the applied field due to the fact that the measured anisotropy energy along the *a* axis is more than four times as high as that along the *b* axis. The self-reversibility was facilitated by substrate-imposed stresses which resisted the reorientation process.[21]

Here, we present a study of the temperature-dependent MIR effect for [101]-oriented $Ni_{51}Mn_{29}Ga_{20}$(at. %) films deposited on YSZ substrates.[19] The films show a partial self-reversible MIR effect similar to that observed in the

literature.[16,17,19,20] Through an analysis of the MIR response, combined with a detailed characterization of the film's crystallographic texture, microstructure, and magnetic domain structure, it is concluded that the aforementioned mechanism describing the MIR effect in {100} Ni-Mn-Ga films[16] cannot be applied to the present situation. We propose an alternative mechanism able to account for the observed phenomena. Also reported is the temperature dependency of the MIR process for thin films in the range of 100–340 K. The dependency, which has never been characterized for thin films, follows a similar trend to what is being observed in single crystals,[10,14] whereby lower temperatures require a higher magnetic activation field. However, the critical fields needed to activate the MIR process over the entire temperature range are found to be significantly lower for the thin films than those required for single crystals.

II. EXPERIMENTAL

A procedure for the epitaxial growth of Ni-Mn-Ga films using the pulsed laser deposition technique was described elsewhere.[19] $Ni_{51}Mn_{29}Ga_{20}$(at. %) films, with a thickness of 250 nm, were grown on (001) YSZ substrates at 625 °C under a 10^{-7} Torr vacuum environment. The relatively high growth temperatures became accessible through the use of a target material enriched with both manganese and gallium to compensate for the loss of these elements during deposition due to their high elemental vapor pressures. The films showed a high degree of crystallinity with the micrometer-sized grains and the desired highly twinned microstructure for the martensitic phase at room temperature. The films used in the present study have a higher degree of in-plane grain alignment, yielding superior diffraction data than the previously reported films.[19] The three-dimensional x-ray diffraction (XRD3) carried out at room temperature reveals the presence of four orientations of the orthorhombic martensitic phase in the films with lattice parameters $a=6.112(4)$ Å, $b=5.885(3)$ Å, and $c=5.527(2)$ Å. The diffraction data set obtained at 380 K indicates a cubic austenitic phase with $a=b=c=5.846(3)$ Å.

The deposited films have undergone a characterization process using various techniques which have explored the transport, magnetic, crystallographic, and microstructural properties. The θ-2θ x-ray spectrometry and the three-dimensional x-ray diffractometry indicate a highly textured film growing along the [101] direction. The temperature-dependent x-ray measurements also reveal that films undergo a reversible martensitic transformation between 307 and 370 K. The phase transition temperatures M_s, M_f, A_s, and A_f, defining the start and finish temperatures for the forward and reverse martensitic transformations, were determined by the temperature-dependent dc resistivity measurement as $M_s=361$ K, $M_f=307$ K, $A_s=312$ K, and $A_f=370$ K. Coinciding with the structural phase transition was ferromagnetic ordering occurring over a temperature interval ranging from 359 to 352 K upon cooling.[19,22]

The magnetization measurements were carried out on the films using a Quantum Design magnetic property measurement system associated with the superconducting quantum interference device. XRD3 techniques were used to study the crystallographic texture. These measurements were performed with a Rigaku RU-200 rotating anode Cu $K\alpha$ x-ray generator, on a Bruker 3-circle D8 goniometer with parallel-focusing mirror optics and a Bruker Smart 6000 CCD detector. ω and φ scans were used to generate the three-dimensional diffraction pattern. The scans were carried out with a 0.5° scan step and 2 s exposure times at a sample-detector distance of 5.178 cm. The range of the scan angles is listed in Table I. The unit cells of the martensitic and austentic phases were indexed using SMART and RLATT programs from Bruker-AXS (Ref. 23) and the MAX3D (Ref. 24) software package. Pole figures were generated with Bruker GADDS (Ref. 23) software. Studies of the magnetic domain structure of the films were carried out with magnetic force microscopy (MFM) using a Digital Instrument scanning probe microscope and a NanoScope IIIa controller. The topography and magnetic force gradient were collected simultaneously using a metal coated etched silicon probe produced by Veeco Instruments Inc., with a lift scan height of 50 nm. The film microstructure was examined with a JEOL 2010 FEG transmission electron microscope (TEM) operating at 200 kV. Other experimental data for these films are available elsewhere.[19,22]

TABLE I. The scan parameters used for collecting the XRD3 data set for $Ni_{51}Mn_{29}Ga_{20}$(at. %) films.

2θ (deg)	ω (deg)	φ (deg)	χ (deg)
−60	170–130	0	54.8
−60	130–170	120	54.8
−60	170–130	240	54.8
−60	170	0–360	54.8

III. RESULTS

In-plane magnetization measurements were used to characterize the magnetic properties of the austenitic and martensitic phases as the temperature was reduced through the magnetic and structural phase transformations. Figure 1 shows the in-plane magnetization loops corresponding to temperatures where there exists (a) pure austenite (372 K), (b) a mixture of austenite and martensite but where the austenite phase dominates (358 K), (c) a mixture of austenite and martensite but where the martensite phase dominates (340 K), and (d) pure martensite (300 K). The magnetic field was applied along the [110] direction of the YSZ substrate, i.e., $H\|[110]_{YSZ}$. At 372 K the magnetization curve exhibits the linear response associated with paramagnetic behavior. As the temperature is lowered to 358 K the film undergoes a ferromagnetic transition of the austenitic phase ($T_c=359$ K), which is accompanied by a significantly broader austenite-to-martensite structural phase transition ($M_s=361$ K).[19,22] Although the ferromagnetic transition leads to a marked increase in magnetization at 358 K compared to the 372 K data, an even greater increase would have been ob-

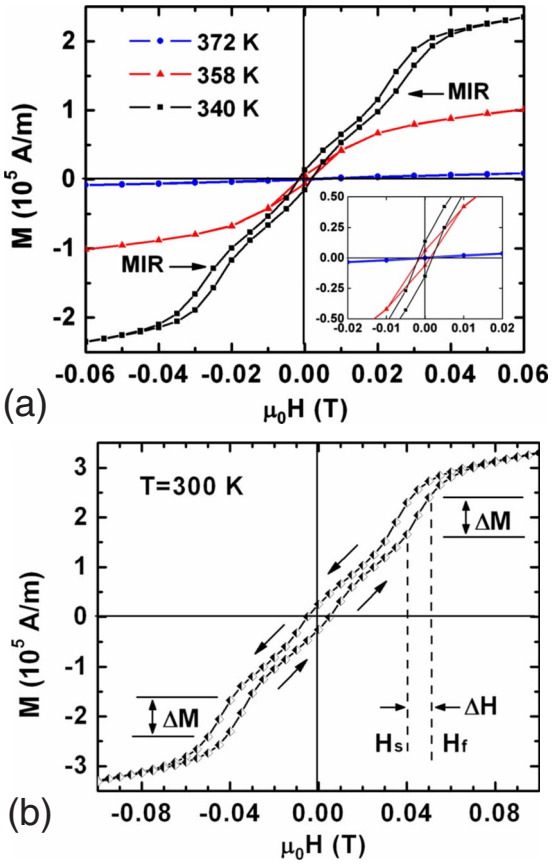

FIG. 1. (Color online) The in-plane magnetization hysteresis loops measured through the structural and magnetic phase transitions at (a) 372, 358, 340 K and (b) 300 K, which correspond to pure austenite (blue circles), a mixture of austenite and martensite but where the austenitic phase is dominant (red triangles), a mixture of both phases but where martensitic phase dominates (black squares), and pure martensite (half white and half black diamonds). The MIR phenomenon, characterized by an abrupt increase in the magnetization, is observed at both 300 and 340 K, where the martensitic phase is either phase pure or predominating. The change in slope is easily recognized as the data points are evenly spaced in the applied magnetic field. The 300 K magnetization data are shown separately in Fig. 1(b) so as to clearly denote the onset (H_s) and completion (H_f) of the activation fields, as well as the magnetization increment (ΔM) induced by the MIR process. Note that the MIR effect is fully reversible. The inset to Fig. 1(a) gives an enlarged view of the magnetization in the vicinity of the origin (i.e., near $\mu_0 H=0$). The magnetic field was applied along the [110] direction of the YSZ substrate, i.e., $H\|[110]_{YSZ}$. The sense of application and removal of the magnetic field is denoted by the arrows in Fig. 1(b).

served if not for the fact that the observed increase is associated with only a partial ferromagnetic ordering. Complete ordering occurs once the sample is cooled to 352 K. In the presence of a weak martensitic component the resulting magnetization at 358 K is thus dominated by the austenitic phase. The film shows the typical ferromagnetic loop with the small coercive field expected for a magnetically soft austenitic phase that exhibits low magnetic anisotropy.[25] At 340 K the martensitic phase has become dominant. The magnetization loop shows a wider hysteresis and a larger coercive field, a response consistent with the high anisotropy of the martensitic phase.[25] Also observed from the 340 K magnetization curve are abrupt changes in slope for magnetic fields near ± 0.025 T, which are apparent in both the magnetizing and demagnetizing processes. Such slope changes are easily recognized since the data points are evenly spaced in the magnetic field ($\mu_0 H$). The changes in slope, which are even more pronounced for the 300 K magnetization data (i.e., for pure martensite), have previously been attributed to the MIR effect.[16,19–21] Of note is that 340 K is the highest temperature where the MIR effect is observed in these $Ni_{51}Mn_{29}Ga_{20}$ films.

During the magnetization process, the 300 K magnetization characteristic [Fig. 1(b)] shows a steeper slope in a field range of 0.04–0.05 T. These magnetic field values, denoted as H_s and H_f, span a range of fields, ΔH, where twin-boundary motion occurs. Such a rise in the slope of the magnetization curve is analogous to the far more abrupt rise observed for single crystals.[10,14] The difference is likely attributed to the crystallographic texture associated with the film, which adds a polycrystalline character[26] to the response. In order to quantize the critical field (H_{MIR}) needed to activate the MIR process, while avoiding the ambiguity associated with the range of magnetic fields over which the effect occurs, we define H_{MIR} as the average of the fields corresponding to the onset and end point of the transition

$$H_{MIR} = \frac{H_s + H_f}{2}.$$

The magnetization increment, ΔM, induced in the entire MIR process is about 17% of the saturation magnetization of 4.2×10^5 A/m. Also evident from the figure is a rapid drop in the magnetization during the demagnetization process. This drop, which corresponds to the restoration of the initial twinning state, also spans a range of magnetic fields, but with an onset that is somewhat lower than H_f. The same phenomenon is also apparent in the third quadrant of the magnetization loop where the magnetic field is applied in the reverse direction. The symmetry in the MIR process implies high twin mobility and a lack of defect pinning sites. Important is the fact that the observed recovery is not reliant on external stimuli as is the case for single crystals, where an external compressive stress applied perpendicular to the magnetic field direction is required to induce the reorientation of the initial twining state after the field is removed.[8–10]

Figure 2 shows the temperature dependence of the activation field, H_{MIR}, for the $Ni_{51}Mn_{29}Ga_{20}$ films. The MIR effect is first observed in the magnetization data at 340 K, where the film contains a significant amount of the martensitic phase. As the temperature is lowered further, the activation field steadily increases, suggesting that it becomes progressively more difficult to activate the MIR process. Such behavior is consistent with that observed for single crystals and has been attributed to a drop in twinning stress at elevated temperatures as well as the increased thermal activation of twin-boundary motion.[10,14,15,27] It has been suggested that the latter effect facilitates the shuffling of atoms in the vicinity of the twin boundary to positions favored by the magnetic

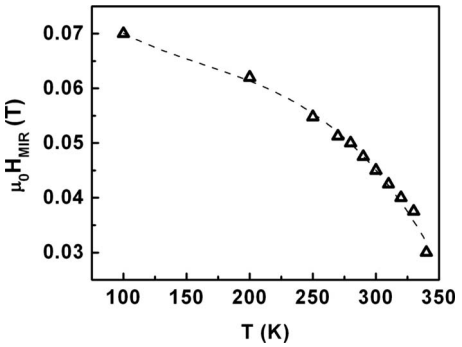

FIG. 2. The critical magnetic field required to activate the MIR process as a function of temperature for a $Ni_{51}Mn_{29}Ga_{20}$ film. H_{MIR} decreases with increasing temperature, a response consistent with a reduction in the twinning stress due to enhanced thermal activation. The dashed line is a guide for the eyes.

field,[27] which would account for the accelerated reduction in the activation field in the range of temperatures between 280 and 340 K. Straka and co-workers[10,14] argued that the influence from the other temperature-dependent magnetic/elastic properties, such as tetragonality (c/a) and the anisotropy constant (K_u), are of less significance.

When analyzing crystallographic data for the Ni-Mn-Ga system, it should be recognized that the unit cell can be defined in a manner which either includes or excludes lattice modulations. The former is often based on the electron[28] or neutron[29] diffraction results, while the latter is usually deduced from XRD (Ref. 30) data. The correlation between the two has been discussed in detail by Pons *et al.*[28] The Miller indices presented here follow the formalism whereby such modulations are excluded.

The XRD3 data set shows a nearly single-phase film with only a few extremely weak peaks which remain unindexed. A comprehensive understanding of the crystallography requires an examination of both the set of {220} and {400} pole figures shown in Figs. 3 and 4, respectively. The (202) pole figure in Fig. 3(a) exhibits a single pole at a 90° radial angle while no such poles are observed for the {220} and {022} pole figures. This indicates that the film is exclusively [101] oriented. The {220} and {022} pole figures each show a ring of eight poles where the rings are at slightly different radial angles (28° and 33°, respectively) due to the orthorhombic nature of the unit cell. The fact that there are eight poles instead of the two expected for a single crystal [shown schematically for the {220} pole figure in Fig. 3(b)] indicates that the film is comprised of four unique in-plane orientations. The azimuthal angle between these orientations is 90° as is depicted schematically in Fig. 3(c). The resulting fourfold symmetry is a reflection of the underlying symmetry of the [001] cubic YSZ substrate. In such a pole pattern, the two {220} poles from orientation 2 [i.e., those labeled as "2" in Fig. 3(a)] can be rotated 180° azimuthal angle into the two {220} poles from orientation 1, indicating the existence of a mirror relationship between these two orientations [i.e., (101) is the mirror plane]. If these two orientations form two sets of martensite variants, then twin pairs will form when one variant lies on top of the other. Such an orientational relationship also exists between orientations 3 and 4. Because no such mirror symmetries exist between orientations offset by 90° azimuthal angle (e.g., between orientations 1 and 3) martensite variants in these orientations cannot share a twinning relationship.

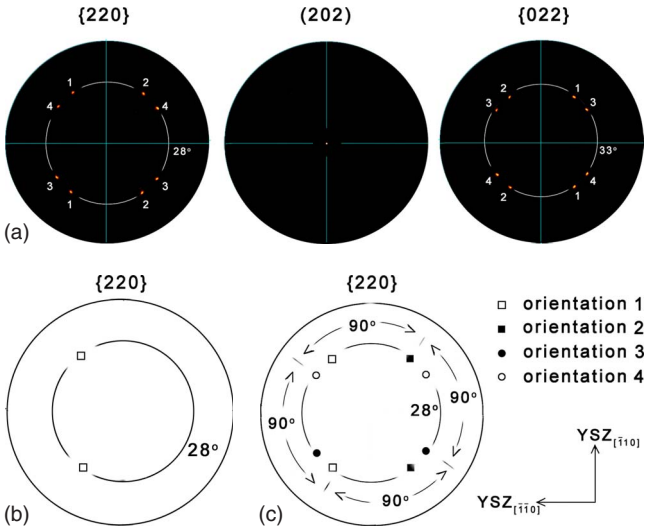

FIG. 3. (Color online) (a) The {220} set of pole figures for the martensitic phase of a $Ni_{51}Mn_{29}Ga_{20}$ film. The observed patterns are consistent with a [101]-oriented film with four in-plane orientations (poles originating from each orientation numbered 1 through 4). (b) A schematic depictions of the {220} pole figure expected for a [101]-oriented single crystal. (c) A schematic depiction of the observed {220} pole figure showing four in-plane crystallographic orientations offset from one another by 90°. The Miller indices at the lower right corner of Fig. 3(c) show the orientation of the YSZ substrate relative to all the pole figures shown.

The {400} pole figures show a result consistent with the {220} pole figures in that the (400) and (004) pole patterns exhibit a fourfold in-plane symmetry, characterized by four (400) and four (004) poles at radial angles of 42.2° and 48.3°, respectively. It should be noted that in the (400) pole figure, only the four poles at a radial angle of 42.2° are associated with the film [i.e., the poles connected with white

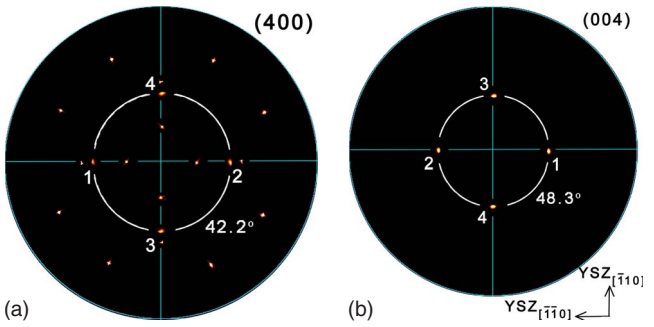

FIG. 4. (Color online) Room-temperature (a) (400) and (b) (004) pole figures for an orthorhombic $Ni_{51}Mn_{29}Ga_{20}$ martensite film. Each pole figure shows four poles connected with white arcs where each pole corresponds to a unique orientation denoted by the numbers 1 through 4. All other major poles in Fig. 4(a) are associated with the (001) YSZ substrate. The Miller indices at the lower right corner of Fig. 4(b) show the orientation of the YSZ substrate relative to all the pole figures shown.

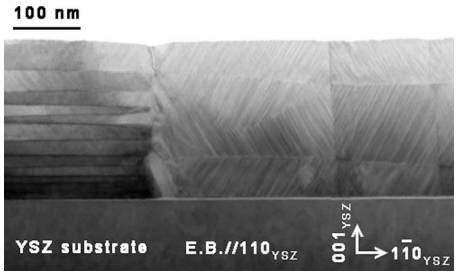

FIG. 5. Bright-field TEM cross-sectional image showing the martensitic microstructure of the $Ni_{51}Mn_{29}Ga_{20}$ film. The image shows three distinct grains each of which is comprised of a series of horizontal plates. Of note is the 2–3-nm-thick feature at the film-substrate interface which is assigned to the austenitic phase. The image was taken with the electron beam parallel to the [110] direction of the YSZ substrate, i.e., E.B.$\|[110]_{YSZ}$. The Miller indices indicating the orientation of the substrate is also provided.

arcs in Fig. 4(a)]. The remaining poles at radial angles of 17.5°, 64.7°, and 35.3° are associated with the {311}/{131}, {113}, and {222} reflections of the YSZ substrate, respectively. The fact that the radial angle between any two poles from the same film orientation is somewhat smaller than 90° indicates that there exists a slight monoclinic distortion to an otherwise orthorhombic unit cell. The experimental (040) pole figure (not shown here) exhibits no poles because the (040) plane of the film is perpendicular to the surface plane of the substrate. Thus, the poles that do exist lie at the experimentally inaccessible edge of the pole figure (i.e., a radial angle of 0°). It should be noted that the four orientations show similar XRD intensities, a clear indication of the equivalent volume fractions occupied by each orientation. Also worth noting is the fact that the XRD3 data set reveals the presence of residual volumes of the austenitic phase (not shown here).

Figure 5 shows a cross-sectional TEM image of the $Ni_{51}Mn_{29}Ga_{20}$ films. The image shows three distinct grains, each of which is highly twinned and comprised of plate-shaped variants. The two rightmost grains are quite similar in appearance, showing inclined thin slices within each martensite plate. These features likely originate from the slip steps formed during the martensitic phase transformation. Such a microstructure results in a further reduction in the transformation strain while maintaining the martensitic crystal structure.[31] The leftmost grain is quite distinctive in appearance, showing no obvious substructures inside the stacked plates. The observation of grains having two distinct morphologies is consistent with the {220} and {400} pole figure results which show in-plane crystallographic orientations offset by 90°. Under such circumstances it is not unexpected for slip steps to be observed for one crystallographic orientation while being absent in a secondary orientation where the diffraction condition is not met. Also apparent in the image is a 2–3 nm interfacial layer which extends across the entire cross-section. If such a layer were of the austenite phase, which persists at room temperature due to substrate clamping effects, it would account for the residual levels of austenite detected in the XRD3 measurements.

Figure 6(a) shows a room-temperature MFM image of the surface of the film. The image shows a spatially intricate

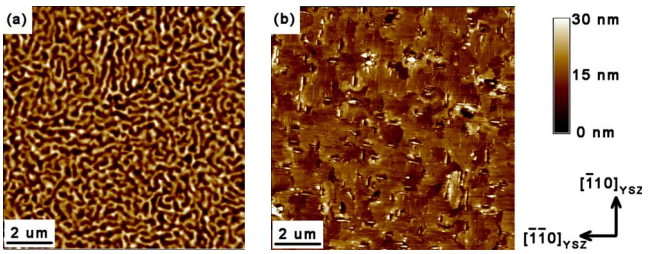

FIG. 6. (Color online) (a) MFM and (b) AFM images for a $Ni_{51}Mn_{29}Ga_{20}$ film showing the magnetic force gradient and surface topography, respectively. Note that the surface topography is not correlated with mazelike magnetic domain pattern. The Miller indices at the lower right corner of Fig. 6(b) show the orientation of the YSZ substrate relative to both images shown.

magnetic domain structure where the out-of-plane component of the magnetization switches from being "in" or "out" of the surface of the film. Figure 6(b) is an atomic force microscopy (AFM) image simultaneously collected from the same area. The results indicate that the mazelike pattern in Fig. 6(a) represents the magnetic microstructure of the film as no similar topological patterns are observed in the film's surface morphology [Fig. 6(b)]. Thus, it is expected that the small length-scale spatial undulation is a manifestation of the magnetization ripples associated with the various variants of this magnetic shape memory alloy. Similar MFM patterns of a rippling of the out-of-plane magnetization component have been observed for (110)-textured Ni-Mn-Ga films grown on Al_2O_3 (Ref. 32) and MgO (Ref. 33) substrates as well as for epitaxial (001) Cu/Ni/Cu multilayers[34] and Ni-rich Ni-Fe thin films.[35]

IV. DISCUSSION

As previously noted, the $Ni_{51}Mn_{29}Ga_{20}$ films studied here exhibit a MIR effect which is different from the corresponding effect observed in single crystals in that: (1) the activation field of 0.03–0.08 T is approximately one third the amplitude of what is required in a single crystal;[10,14] (2) the resultant increment in magnetization is only about 17% of the saturation magnetization whereas for a single crystal it is typically 50% (Refs. 10 and 14); and (3) the MIR process is self-reversible whereas for single crystals it is reversible only under external stimuli.[8–10] It has also been noted that the film's microstructure and texture is strongly influenced by the crystallographic orientation of the substrate material, exhibiting a character that is quite different from that observed for single crystals. The present results suggest that these microstructural properties give rise to a unique magnetic domain pattern which, in turn, manifests itself in a distinctive MIR response, as discussed below.

A detailed understanding of the film's microstructure can be ascertained from a comparison of the crystallographic texture results and the TEM images. The texture indicates that the film is comprised of four different crystallographic orientations, where each orientation has its [101] direction normal to the surface of the substrate but offset by 90° in the film plane. These orientations exhibit a fourfold in-plane

symmetry and are of significance since orientations offset by 90° have no single-crystal analog. This arrangement is, in fact, inherited from the crystallographic texture associated with the austenitic parent phase formed during the deposition process. The parent phase adapts to the underlying fourfold symmetry of the substrate's (001) cubic surface through the formation of two geometrically equivalent grain orientations characterized by $(110)[001]_{\text{austenite}} \| (001)[110]_{\text{substrate}}$ and $(110)[001]_{\text{austenite}} \| (001)[1\bar{1}0]_{\text{substrate}}$, as displayed in Fig. 7(a). The subsequent austenite to martensite phase transformation results in martensite twin variants forming in both grain orientations which gives rise to two additional crystallographic orientations. Variants within the individual grains form twins as shown in Fig. 7(b). This twinning relationship is characterized by a pair of martensitic variants connected by a twin boundary, where the variants appear in the {220} pole figures, or alternatively {400} pole figures, as poles separated by a 180° azimuthal angle (i.e., denoted as orientations 1 and 2 or orientations 3 and 4 in Figs. 3 and 4) with the twin boundary corresponding to the (101) mirror plane. Of crucial importance is the fact that the variants formed within one grain orientation do not share a twinning relationship with variants formed within the other grain orientation because the two sets of perpendicularly oriented grains are inherited from the austenitic phase rather than formed through the martensitic transformation. Such an argument is consistent with the texture results indicating that the crystallographic orientations offset by a 90° azimuthal angle do not show mirror symmetry. This description is consistent with the two unique grain types observed in the TEM cross-sectional image. Also in agreement with this description is the fact that the TEM image shows well-defined straight interfaces between the martensite plates running parallel to the surface of the substrate (see Fig. 5), a feature indicative of the high degree of atomic coherency achieved through a twinning relationship. The fact that these boundaries are parallel to the substrate surface is consistent with the texture results which allow for an intervariant (101) twin plane as is schematically depicted in Fig. 7(b).

The two distinct grain types give rise to unique grain boundaries as is shown in Fig. 5. The leftmost grain boundary, which is somewhat jagged in appearance, occurs when two grains offset by a 90° azimuthal angle meet. The rightmost grain boundary, on the other hand, forms a sharp interface which is nearly normal to the surface of the substrate. This feature is likely the result of a small-angle grain boundary formed between the two like-oriented grains.

With the present understanding of the crystallographic texture and microstructure, it is possible to gain insight into the magnetic microstructure of these films. It should, however, be first mentioned that the easy magnetization axis in an orthorhombic martensite is along the shortest *c* axis of the orthorhombic unit cell, i.e., along [001].[30] In this scenario, it is apparent from Fig. 7(b) that the easy magnetization direction for each variant is neither parallel nor perpendicular to the film's surface, but instead forms the angle θ. For this arrangement the normal component of the magnetization for any particular variant can point either toward the film's surface or away from it. The mazelike appearance of the MFM

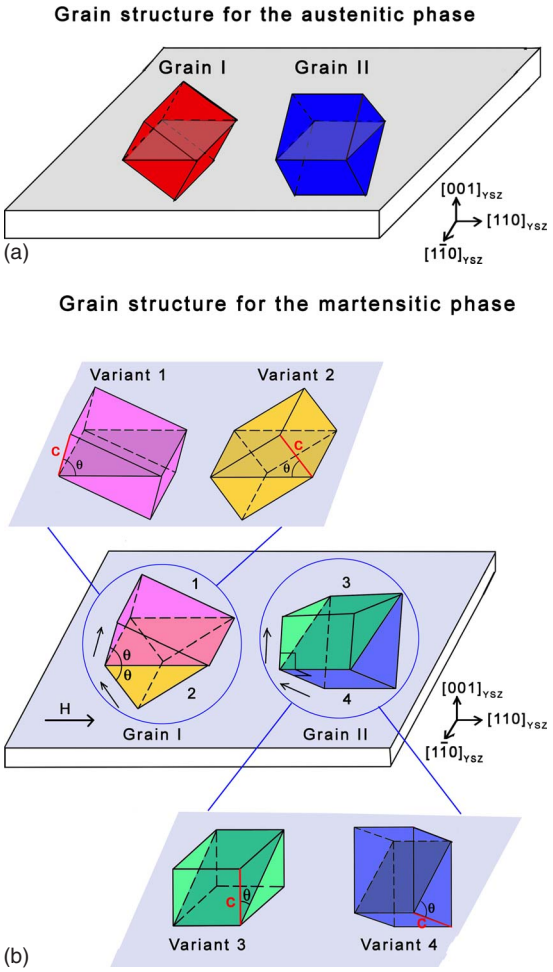

FIG. 7. (Color online) Schematic representation of the grain structure for the (a) austenitic phase and (b) martensitic phase in a $Ni_{51}Mn_{29}Ga_{20}$ film. For the austenitic phase two equivalent grain orientations offset by an in-plane angle of 90° are formed through the adaptation to the substrate's (001) cubic surface. The subsequent martensitic transformation leads to twin variants generated in each grain orientation. Variants 1 and 2 form a twin pair within grain I while the variants 3 and 4 share a twinning relationship within grain II. The twin boundary which connects the two twin variants is the (101) plane of the unit cell. The crystallographic orientation of each individual variant is also shown. Unique to each orientation is its *c*-axis direction which is colored in red. The variants are numbered 1 through 4 in (b). The direction of the applied magnetic field as well as the magnetization direction for each variant is denoted by an arrow. The Miller indices at the lower right corner of both (a) and (b) show the orientation of the YSZ substrate relative to all the martensitic variants shown.

image [Fig. 6(a)] is consistent with these arguments as an undulation in the magnetization could effectively reduce the magnetostatic energy through the formation of a ripple domain structure.[34–37] It should be noted that although the magnetization of these variants are denoted by an upward pointing arrow, it is equally likely that the magnetization direction could also point downward, as is apparent from the ripple domain structure. One can expect that to avoid generating poles at the twin boundary, the two twin-related variants

within grain I or grain II should have their magnetization directions pointing both up or both down.

The in-plane magnetization hysteresis loops, shown in Fig. 1, reveal that the films exhibit a reversible MIR effect, which is similar to that observed for {100} oriented orthorhombic Ni-Mn-Ga films.[16] For this effect to be observed, there must exist a mechanism for promoting reversibility as well as a means by which a reorientation of variants can occur while keeping the film clamped to the underlying substrate. As mentioned in the introduction, the self-reversibility for the MIR effect in a {100}-oriented film was attributed to substrate-imposed stresses that developed during the reorientation of the in-plane lattice constants of an orthorhombic unit cell.[16,21] These stresses force the film back to its initial state once the field is removed. While this provides a description of the MIR effect in the {100}-oriented films presented by Thomas *et al.*,[16] the same description cannot be applied to the behavior observed for the [101] films studied here. This is a consequence of the fact that the two twin-related variants which convert from one to the other, have an identical epitaxial relationship with the substrate, i.e., $(101)[010]_{film} \| (001)[1\bar{1}0]_{\text{substrate}}$ for variants 1 and 2 and $(101)[010]_{film} \| (001)[110]_{\text{substrate}}$ for variants 3 and 4, as shown in Fig. 7(b). Thus, when variants 1 and 2 (or alternatively variants 3 and 4) switch from one to the other, no change is required in the in-plane lattice parameters and, as a result, no substrate-imposed stresses will develop. The presence of the 2–3-nm-thick austenite layer at the substrate-film interface (Fig. 5) should also help facilitate the MIR process as the layer disconnects the martensite variants from the underlying substrate. As a result, the stresses imposed by the substrate on the martensite grains above the austenite layer are expected to be significantly smaller. In the absence of the substrate-imposed stresses a [101] single-crystal film should behave exactly as a single crystal, showing a complete MIR effect which does not display self-reversibility. The fact that a reversible MIR effect is observed requires that a different mechanism comes into play for these [101]-oriented Ni-Mn-Ga films. An analysis of the response of the individual variants to an externally applied field reveals that the microstructure itself is the most likely origin of the reversibility.

Labeled on Fig. 7(b) is the direction of the externally applied magnetic field, i.e., $H \| [110]_{\text{YSZ}}$, relative to the four crystallographically oriented variants. Immediately evident is the fact that the magnetic field direction relative to the magnetization direction varies between variants and in no case are the two directions ever parallel. It is apparent from an examination of the magnetization direction labeled on the individual variants that the magnetization of only one of the two twin-related variants in grain I has a component parallel to the external field [e.g., variant 1 in Fig. 7(b)]. This component makes this variant more favorable than its twin-related counterpart whose same magnetization component is antiparallel to the field. A preferential field selection, however, is not expected to occur between variants 3 and 4 since neither shows a magnetization component in the direction of the magnetic field. The arrangement described will inevitably lead to a spatially varying MIR response which is dependent on the local microstructural and crystallographic environment.

For the scenario where there exists a twin boundary between variants 1 and 2 [grain I in Fig. 7(b)], there will exist a difference in the Zeeman energy between these variants which is given by

$$\Delta E = 2\mu_0 M_s H \cos\theta,$$

where μ_0 is the magnetic permeability of free space and M_s is the saturation magnetization, H is magnetic field and θ is the angle between the magnetization direction for a variant and the magnetic field. This difference in energy results in the application of a pressure on the twin boundary which, for fields in excess of H_{MIR}, can drive the twin-boundary motion in a manner that favors variant 1 at the expense of variant 2. A similar situation has been discussed by O'Handley[38] who pointed out that the field-induced twin-boundary motion occurs when strong magnetic anisotropy is present. If the Zeeman energy is much smaller than the magnetic anisotropy (i.e., $M_s H/2K_u \leq 1$) then the effect of the field is to move the twin boundaries rather than to rotate the magnetization within unfavorably oriented variants. In an effort to examine whether the films presented here belong to this category, we estimated the Zeeman energy, $M_s H$, for a MIR-activation field of $\mu_0 H_{\text{MIR}} = 0.045$ T and a saturation magnetization of 4.2×10^5 A/m at 300 K. For this scenario, the value of the Zeeman energy is on the order of 10^4 J/m^3. This value is an order of magnitude smaller than the magnetic anisotropy energy, K_u, which is on the order of 10^5 J/m^3 (Ref. 39). This result indicates that the strong anisotropy assumption used for the films presented in this report is reasonable. The elastic energy introduced by the twin-boundary motion, $\sigma\varepsilon/2$, is also estimated for a twinning stress of 2 MPa (Ref. 39) and a 5% strain. While a 10% strain is theoretically predicted for a single crystal with similar lattice parameters (i.e., $c/a = 0.9$) upon completion of the MIR process from the single-variant state with a field applied parallel to the hard [100] axis, the 5% value used here is a more reasonable estimation. This reduced value takes into account such factors as the twin variants existing in these textured films before the onset of the MIR process and that the magnetic field was applied parallel to the twin boundary instead of being parallel to the magnetization direction of one of the two variants. The calculation indicates that the elastic-energy density is also on the order of 10^4 J/m^3, as is the case for the Zeeman energy. This implies that with an applied field of 0.045 T it is possible to induce twin-boundary motion. O'Handley[38] has determined that the magnetic driving force on the twin boundary is strongest when the external field is applied parallel to the twin boundary and bisects the angle between the magnetization of the twin variants under consideration. This geometry accurately describes the case presented here. It is also evident that magnetic domain-wall motion is absent during the magnetic field-induced twin-boundary motion in the Ni-Mn-Ga system.[40] Considering all these aspects, the MIR effect observed here is very likely induced by the Zeeman-energy difference between the two twin-related variants.

It should be understood that the aforementioned reorientation mechanism is not possible in the second scenario (i.e., for variants in grain II) shown in Fig. 7(b). In this case, both variants [i.e., variants 3 and 4 in Fig. 7(b)] have their c axes

perpendicular to the magnetic field direction and, hence, do not experience any difference in Zeeman energies. As a result, there is no incentive to convert from one orientation to the other through twin-boundary motion. It is also considered unlikely that the variants in grain II experience any MIR effect as a result of being in contact with a variant from grain I, because there is no twinning relationship between them. Thus the geometrical arrangement of the grain orientations results in 50% of the film's grains being able to participate in the MIR process (i.e., MIR active) and 50% of the film's grains being MIR inactive. It should be understood, however, that the inactive variants possess all of the material properties necessary to become MIR active, as the inactivity arises solely from their crystallographic orientation relative to the applied magnetic field. For the MIR-active grains, one of the two variants will be oriented favorably with respect to the field while the other will have an incentive to reorient when the magnetic field is applied, resulting in a maximum of 25% of the film variants reorienting.

The presence of these MIR-inactive variants also accounts for the small increase in magnetization during the reorientation process when compared to single crystals. The fact that the magnetic reorientation is confined to pre-existing twin-related variants within individual grains accounts for the relatively small MIR activation field compared to the field reported for single crystals. By contrast, the samples used in the single-crystal experiments were magnetically or mechanically forced to become a single variant in order to achieve the maximum possible strain from the MIR effect.[8–10] In this case the activation field must be large enough to provide the nucleation energy to first produce the twins and then to overcome the stresses induced by the twin-boundary motion. The experiments with thin films described here are more akin to stress-induced elastic twinning observed for calcite, where the initial nucleation step was bypassed, which resulted in the deformation being realized using a much smaller load.[41]

While only 50% of the grains are active in the magnetic reorientation process, the other 50% are not considered to be completely passive in nature. During the process of twin-boundary motion, the atoms in the reoriented variants undergo twinning shear along the $[10\bar{1}]$ direction, a direction parallel to the substrate's surface, e.g., the $[10\bar{1}]$ shear direction of the atoms in variant 2 in the MIR-active grain I is parallel to the [110] direction of the YSZ substrate, as shown in Fig. 7(b). Such twinning shear in the active grains must be accommodated by the elastic distortion of inactive grains [e.g., grain II in Fig. 7(b)]. This will lead to the development of large elastic stresses in the inactive grains, making them plastically "hard" elements within the substructure of the film. With no effective means by which to relieve these stresses it is expected that the atoms in active grains are forced back to their initial positions when the external magnetic field is removed. Such a partition of stress between a "hard" parent phase and a "soft" twin has recently been observed using three-dimensional x-ray diffraction in magnesium alloys subjected to compressive loading.[42] In addition, reversibility of the twinning transformation has been observed in bulk polycrystalline samples of Ni-Mn-Ga where the phenomenon was attributed to a restoring force arising from differently oriented crystallites.[26] In contrast to the polycrystalline material, the highly textured films appear to be far more effective in the reorientation process, displaying a larger magnetization increment that is induced by a smaller magnetic field. Within this framework a [101]-oriented film without MIR-inactive grains should be capable of producing a more complete MIR effect, but the effect would not be completely self-reversible.

Present results suggest that the substrate plays a crucial role in determining the initial crystallographic texture and microstructure, but plays a more passive role in controlling the MIR response. The existence of the in-plane grain orientations offset by 90° is a consequence of the adaptation of the [110]-oriented Ni-Mn-Ga austenitic parent phase to the four-fold symmetry of the YSZ substrate's (001) cubic surface. During the subsequent austenite to martensite phase transformation, the substrate's constraints to the austenite lattice lead to a 2–3-nm-thick residual austenite layer at the film-substrate interface. It suggests that, while the substrate must hinder the degree of atomic shuffling during the martensitic phase transformation the stresses imposed on the martensitic grains above the austenitic layer are significantly weakened. Interfacial stresses are sufficiently relieved through various strain relaxation mechanisms such as dislocations and the grain boundaries. Once the stresses are relieved the substrate becomes less of a factor. This, combined with the fact that each of the four crystallographic orientations share an identical epitaxial relationship with the substrate, makes it highly unlikely that the substrate is producing any appreciable stresses while one variant converts to the other. On the contrary, the shearing of the atoms during twin-boundary movement is strongly inhibited at the boundaries between the MIR-active and inactive grains. It is the initial formation of these structures during film growth where the substrate must play a decisive role. This leads to the intriguing possibility of engineering a desired response based on an appropriately chosen substrate material, through graphoepitaxy, or through the promotion of a step-flow growth mode facilitated by a miscut substrate. Successful implementation of such strategies could lead to the ability to tune the film's structural and magnetic microstructure toward a particular application where, for example, MIR-inactive grains could be included or excluded to achieve either self-activated reversibility or allow a more complete, but irreversible, MIR effect.

V. CONCLUSION

We have examined the isothermal and temperature-dependent magnetization properties for [101]-oriented $Ni_{51}Mn_{29}Ga_{20}$ films deposited on (001) YSZ substrates and described the observed MIR effect within the context of the film's crystallographic texture, microstructure, and magnetic domain arrangement. The MIR response of these films is decidedly different from their single-crystal counterpart, displaying both a lower activation field and a self-activated reversibility. These distinctions are attributed to a characteristic film texture, which is a product of substrate-imposed symmetries. The lower activation field is accounted for by the

presence of pre-existing twin structures within individual grains, which more readily respond to the applied magnetic field. The reversibility cannot be attributed to substrate imposed stresses as is the case for [100]-oriented films, but instead originates from elastic energy and a mechanical restoring force imposed by the 50% of the MIR-inactive grains. Both of these properties are of significance to potential device applications where reversibility and actuation at low fields are desirable.

ACKNOWLEDGMENTS

The authors acknowledge the Natural Sciences and Engineering Research Council of Canada (NSERC), the Ontario Centres of Excellence, and the Canadian Institute for Advanced Research (CIFAR) for funding and the Canadian Centre for Electron Microscopy (CCEM) for access to their facilities. P. Dube and A. Duft are acknowledged for their assistance with sample characterization.

*Present address: Department of Mechanical Engineering, Temple University, 1947 N. 12th Street, Philadelphia, PA 19122.
†niewczas@mcmaster.ca

[1] K. Ullakko, J. K. Huang, C. Kantner, R. C. Ohandley, and V. V. Kokorin, Appl. Phys. Lett. **69**, 1966 (1996).
[2] O. Heczko, J. Magn. Magn. Mater. **290-291**, 787 (2005).
[3] A. Sozinov, A. A. Likhachev, N. Lanska, and K. Ullakko, Appl. Phys. Lett. **80**, 1746 (2002).
[4] S.-E. Park and T. R. Shrout, J. Appl. Phys. **82**, 1804 (1997).
[5] F. Li, Z. Xu, X. Wei, X. Yao, and L. Jin, Appl. Phys. Lett. **93**, 192904 (2008).
[6] M. Pasquale, Sens. Actuators, A **106**, 142 (2003).
[7] T. Kakeshita and K. Ullakko, MRS Bull. **27**, 105 (2002).
[8] S. J. Murray, M. Marioni, S. M. Allen, R. C. O'Handley, and T. A. Lograsso, Appl. Phys. Lett. **77**, 886 (2000).
[9] L. Straka and O. Heczko, J. Magn. Magn. Mater. **290-291**, 829 (2005).
[10] L. Straka, O. Heczko, and S. -P. Hannula, Scr. Mater. **54**, 1497 (2006).
[11] M. Pasquale, C. P. Sasso, S. Besseghini, E. Villa, and V. Chernenko, J. Appl. Phys. **91**, 7815 (2002).
[12] Z. H. Liu, M. Zhang, W. Q. Wang, W. H. Wang, J. L. Chen, G. H. Wu, F. B. Meng, H. Y. Liu, B. D. Liu, J. P. Qu, and Y. X. Li, J. Appl. Phys. **92**, 5006 (2002).
[13] W. H. Wang, G. H. Wu, J. L. Chen, S. X. Gao, W. S. Zhan, G. H. Wen, and X. X. Zhang, Appl. Phys. Lett. **79**, 1148 (2001).
[14] O. Heczko and L. Straka, J. Appl. Phys. **94**, 7139 (2003).
[15] B. W. Peterson, S. M. Allen, and R. C. O'Handley, J. Appl. Phys. **104**, 033918 (2008).
[16] M. Thomas, O. Heczko, J. Buschbeck, U. K. Rössler, J. McCord, N. Scheerbaum, L. Schultz, and S. Fähler, New J. Phys. **10**, 023040 (2008).
[17] O. Heczko, M. Thomas, J. Buschbeck, L. Schultz, and S. Fähler, Appl. Phys. Lett. **92**, 072502 (2008).
[18] C. A. Jenkins, R. Ramesh, M. Huth, T. Eichhorn, P. Pörsch, H. J. Elmers, and G. Jakob, Appl. Phys. Lett. **93**, 234101 (2008).
[19] Y. Zhang, R. A. Hughes, J. F. Britten, W. Gong, J. S. Preston, G. A. Botton, and M. Niewczas, Smart Mater. Struct. **18**, 025019 (2009).
[20] J. Buschbeck, R. Niemann, O. Heczko, M. Thomas, L. Schultz, and S. Fähler, Acta Mater. **57**, 2516 (2009).
[21] M. Thomas, O. Heczko, J. Buschbeck, L. Schultz, and S. Fähler, Appl. Phys. Lett. **92**, 192515 (2008).
[22] Y. Zhang, R. A. Hughes, J. F. Britten, P. Dube, J. S. Preston, G. A. Botton, and M. Niewczas (unpublished).
[23] BRUKER AXS, http://www.bruker-axs.com/
[24] J. F. Britten and W. Guan, Compcomm Newsletter of the International Union of Crystallography Commission on Crystallography Computing (IUCr) **8**, 96 (2007).
[25] R. Tickle and R. D. James, J. Magn. Magn. Mater. **195**, 627 (1999).
[26] J. Gutiérrez, J. M. Barandiarán, P. Lázpita, C. Seguí, and E. Cesari, Sens. Actuators, A **129**, 163 (2006).
[27] R. C. O'Handley, D. I. Paul, S. M. Allen, M. Richard, J. Feuchtwanger, B. Peterson, R. Techapiesaňcharoenkij, M. Barandiarán, and P. Lázpita, Mater. Sci. Eng., A **438-440**, 445 (2006).
[28] J. Pons, V. A. Chernenko, R. Santamarta, and E. Cesari, Acta Mater. **48**, 3027 (2000).
[29] P. J. Brown, J. Crangle, T. Kanomata, M. Matsumoto, K.-U. Neumann, B. Ouladdiaf, and K. R. A. Ziebeck, J. Phys.: Condens. Matter **14**, 10159 (2002).
[30] A. Sozinov, A. A. Likhachev, and K. Ullakko, IEEE Trans. Magn. **38**, 2814 (2002).
[31] H. K. D. H. Bhadeshia and R. W. K. Honeycombe, *Steels: Microstructure and Properties* (Butterworth-Heinemann Elsevier, Oxford, 2006).
[32] V. A. Chernenko, R. L. Anton, M. Kohl, M. Ohtsuka, I. Orue, and J. M. Barandiaran, J. Phys.: Condens. Matter **17**, 5215 (2005).
[33] V. A. Chernenko, R. L. Anton, J. M. Barandiaran, I. Orue, S. Besseghini, M. Ohtsuka, and A. Gambardella, IEEE Trans. Magn. **44**, 3040 (2008).
[34] R. C. O'Handley, *Modern Magnetic Materials: Principles and Applications* (John Wiley & Sons, New York, 2000).
[35] N. Saito, H. Fujiwara, and Y. Sugita, J. Phys. Soc. Jpn. **19**, 421 (1964).
[36] R. J. Spain, Appl. Phys. Lett. **3**, 208 (1963).
[37] A. Hubert and R. Schafer, *Magnetic Domains—The Analysis of Magnetic Microstructures* (Springer, New York, 1998).
[38] R. C. O'Handley, J. Appl. Phys. **83**, 3263 (1998).
[39] O. Söderberg, Y. Ge, A. Sozinov, S. –P. Hannula, and V. K. Lindroos, Smart Mater. Struct. **14**, S223 (2005).
[40] Y. W. Lai, N. Scheerbaum, D. Hinz, O. Gutfleisch, R. Schäfer, L. Schultz, and J. McCord, Appl. Phys. Lett. **90**, 192504 (2007).
[41] A. J. Williams and R. W. Cahn, in *Deformation Twinning*, Proceedings of the Metallurgical Society Conferences, edited by R. E. Reed-Hill, J. P. Hirth, and H. C. Rogers (Gordon and Breach Science, Gainesville, Florida, 1963), Vol. 25, p. 192.
[42] C. C. Aydıner, J. V. Bernier, B. Clausen, U. Lienert, C. N. Tomé, and D. W. Brown, Phys. Rev. B **80**, 024113 (2009).